

Experimental observation of the spin-Hall effect in a two dimensional spin-orbit coupled semiconductor system

J. Wunderlich,¹ B. Kästner,^{1,2} J. Sinova,³ and T. Jungwirth^{4,5}

¹*Hitachi Cambridge Laboratory, Cambridge CB3 0HE, UK*

²*National Physical Laboratory, Teddington T11 0LW, UK*

³*Department of Physics, Texas A&M University, College Station, TX 77843-4242, USA*

⁴*Institute of Physics ASCR, Cukrovarnická 10, 162 53 Praha 6, Czech Republic*

⁵*School of Physics and Astronomy, University of Nottingham, Nottingham NG7 2RD, UK*

(Dated: February 2, 2008)

We report the experimental observation of the spin-Hall effect in a two-dimensional (2D) hole system with Rashba spin-orbit coupling. The 2D hole layer is a part of a p-n junction light-emitting diode with a specially designed co-planar geometry which allows an angle-resolved polarization detection at opposite edges of the 2D hole system. In equilibrium the angular momenta of the Rashba split heavy hole states lie in the plane of the 2D layer. When an electric field is applied across the hole channel a non zero out-of-plane component of the angular momentum is detected whose sign depends on the sign of the electric field and is opposite for the two edges. Microscopic quantum transport calculations show only a weak effect of disorder suggesting that the clean limit spin-Hall conductance description (intrinsic spin-Hall effect) might apply to our system.

PACS numbers: 75.50.Pp, 85.75.Mm

The Hall effects are among the most recognized families of phenomena in basic physics and applied microelectronics. The ordinary and quantum Hall effects, which, e.g., proved the existence of positively charged carriers (holes) in semiconductors and led to the discovery of fractionally charged quasiparticles [1], occur due to the Lorentz force that deflects *like-charge* carriers towards one edge of the sample creating a voltage transverse to the current. In the anomalous Hall effect [2], the spin-orbit interaction plays the role of the force that deflects *like-spin* carriers to one edge and opposite spins to the other edge of the sample. In a ferromagnetic material this leads to a net charge imbalance between the two sides which allows to detect magnetization in the conductor by simple electrical means. Here we report the experimental observation of a new member of the Hall family - the spin-Hall effect (SHE). As an analogue of the anomalous Hall effect but realized in non-magnetic systems the SHE opens new avenues for inducing and controlling spin-currents in semiconductors without applying magnetic fields or introducing ferromagnetic elements.

Predictions of the SHE were reported, within different physical contexts, in several seminal studies [3, 4, 5, 6] and currently its microscopic origins are subject of an intense theoretical debate [7, 8, 9, 10, 11, 12, 13, 14, 15, 16, 17, 18]. Experimentally, the SHE has been elusive because in non-magnetic systems the transverse spin-currents do not lead to net charge imbalance across the sample, precluding the simple electrical measurement. To demonstrate the SHE, we have developed a novel p-n junction light emitting diode (LED) microdevice, in a similar spirit to the one proposed in Ref. 5 but distinct in that it couples two dimensional hole and electron doped

systems. Its co-planar geometry and the strong spin-orbit (SO) coupling in the embedded two-dimensional hole gas (2DHG), whose ultra-small thickness deminishes current induced self-field effects, are well suited for inducing and detecting the SHE. When an electric field is applied across the hole layer, a non zero out-of-plane component of the spin is optically detected whose sign depends on the sign of the field and is opposite for the two edges, consistent with theory predictions.

The LEDs were fabricated in (Al,Ga)As/GaAs heterostructures grown by molecular-beam epitaxy and using modulation donor (Si) and acceptor (Be) doping in (Al,Ga)As barrier materials. The planar device features were prepared by optical and electron-beam lithography. Schematic of the wafer and numerical simulations of conduction and valence band profiles are shown in Fig. 1(a,b) [20]. Two wafers were investigated that differ in the 3 nm undoped $\text{Al}_x\text{Ga}_{1-x}\text{As}$ spacer at the upper interface, with wafer 1 having $x = 0.5$ and wafer 2 $x = 0.3$. The heterostructures are p-type; the band-bending leads to the formation of an empty triangular quantum well in the conduction band at the lower interface and an occupied triangular quantum well near the upper interface, forming a 2DHG. The co-planar p-n junction is created by removing acceptors from a part of the wafer by etching, leading to population of the previously depleted conduction band well and depletion of the 2DHG in that region. The diode has a rectifying $I-V$ characteristic and the onset of the current is accompanied by electro-luminescence (EL) from the p-region near the junction step edge [20]. The current, $I_{LED} \approx 100\mu\text{A}$, is dominated by electrons moving from the n- to p-region; the opposite hole current is negligibly small due to lower mobility of holes [20].

The interpretation of EL peaks shown in Fig. 1(c,d)

starts from a comparison with measured photoluminescence (PL). Following previous PL studies [21, 22] of (Al,Ga)As/GaAs single-heterojunctions, we assign the sharp high energy PL peaks (X) to well known GaAs exciton lines, and the lower energy peaks (I) to 2DEG to acceptor or donor to 2DHG transitions. The other PL recombination process identified previously in literature [21, 22], that involves 3D electron to 2D hole transition in the p-region (or the analogous process in the n-region), is unlikely to contribute to our PL spectra due to the large built-in electric field in the unbiased structure.

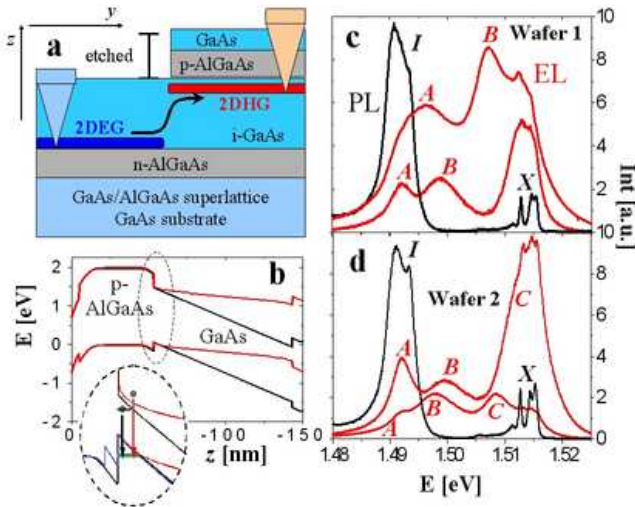


FIG. 1: Basic characteristics of the LED. (a) The schematic cross-section of the co-planar p-n junction LED device. At forward bias of order of the GaAs band-gap, electrons move from the 2DEG to the 2DHG where they recombine. The highest intensity of the emitted light is in the p-region near the junction step-edge. (b) Numerical simulations of the conduction and valence band profiles along the $\langle 001 \rangle$ growth direction (z -axis) in the un-etched part of the wafer near the step edge. Black lines correspond to an unbiased p-n junction and red lines to a forward bias of 1.5 V across the junction. In the detailed image of the upper (AlGa)As/GaAs interface (with the conduction band shifted down in energy for clarity) we indicated possible sub-GaAs-gap radiative recombinations with the 2DHG involving either 3D electrons in the conduction band (red arrow) or impurity states (black arrow). Black line corresponds to unbiased wafer 1 and blue line to wafer 2. (c,d) Photoluminescence spectra (black) and electro-luminescence spectra (red) at low (lower curves) and high (higher curves) bias measured in wafer 1 and 2 at 4.2 K. Impurity (I), excitonic (X), and 3D electron to 2D hole transitions (A , B , C) are identified. We focus on peak B which has small overlap with the I and X lines.

In the EL spectra, the excitonic peaks are clearly visible and, consistently, their position is independent of wafer and applied p-n junction bias. A non-zero EL spectral weight at peaks I suggests that recombination processes with impurity states may contribute in the low energy part of EL. The peaks I are expected to shift to

lower energies under forward bias because of the weaker confinement at the interfaces. Therefore, EL in the spectral range between the PL I and X peaks originates from another mechanism, i.e., from the 3D electron to 2D hole recombination. The broad peak B is the most striking example of such a process. Additional related peaks, A and C , can be identified in wafer 1 at high bias or in wafer 2 at low bias, respectively. These EL peaks shift to higher energies with increasing I_{LED} , which is reminiscent of the behavior of 3D electron to 2D hole transition peaks as a function of the excitation power, reported in the PL measurements in single AlGaAs/GaAs heterojunctions [21].

Fig. 2(a) presents our microscopic calculations of the 2DHG energy structure [23]. The confining potential of the unbiased wafer 1 was assumed in these numerical simulations. Only one heavy-hole (HH) and one light-hole (LH) bound state forms in the quantum well. The calculated spin orientation as a function of the wavevector component k_y parallel to the I_{LED} is plotted in Fig. 2(b). Near $\mathbf{k} = 0$, the HH subband states with total angular momentum $j_z = \pm 3/2$ are split from the LHs with $j_z = \pm 1/2$ due to different HH and LH effective masses, which forces the HH spins to align with the z -axis. (Note that in the 4-band representation of the valence band states [23] the total angular momentum and spin operators of holes are related as $\mathbf{j} = 3\mathbf{s}$.) For larger wavevectors, the mixing with LH states together with the Rashba type of the SO interaction in the asymmetric quantum well [23] result in the splitting of the HH subband and in a vanishingly small angular momentum component $\langle s_z \rangle$. The non-zero in-plane component of spin is oriented perpendicular to the 2D \mathbf{k} -vector. For the measured hole density, $p_{2D} = 2 \times 10^{12} \text{ cm}^{-2}$, only the HH 2D subband is occupied by holes.

Assuming that the optical recombination is dominated by states close the hole subbands Fermi wavevectors [22] and realizing that the 3D electron bands occupation under forward bias is strongly asymmetric along k_y , we can now assign peaks A and B to hole transitions to the split HH subbands. Peak C is assigned to the LHs which may become populated in biased wafer 2 due to a weaker 2DHG confinement, compared to the one considered in Fig. 2. For simplicity we now focus on peak B where the role of impurity and exciton recombinations can be safely neglected.

The detection of spin-polarization phenomena is done by measuring circular polarization (CP) of the light. Due to optical selection rules, a finite CP along a given direction of the propagating light indicates a finite spin-polarization in this direction of carriers involved in the recombination. In Fig. 2(c,d) we plot the CP of peak B for light detection axis close to the 2DHG plane and perpendicular to I_{LED} . The non-zero CP detected in the absence of an external magnetic field, consistent with the results in Fig. 2(b), is an experimental demonstration of a

spin-polarization effect induced by asymmetric band occupation [24]. Data taken at finite magnetic field applied along the x-direction show the expected [23] cooperative or competing effects of the field and the Rashba SO coupling, depending on the sign of the field. Comparison between these data and data in Fig. 2(e,f), showing CP measurement at magnetic fields and light detection axis along the z-direction, confirm the strongly anisotropic Landé g-factor typical of the Rashba SO coupled 2DHG [23]. Fig. 2(e,f) confirms that the CP is purely in-plane at zero external magnetic field which is a crucial piece of evidence in the demonstration of the SHE, which we now discuss.

In the SHE, non-zero $\langle s_z \rangle$ occurs as a response to external electric field and the carries with opposite spins are deflected to opposite edges of the sample parallel to the SHE driving electrical current. A microdevice that allows us to induce and detect such a response is shown in Fig. 3(a). A p-channel current, $I_p \approx 100 \mu\text{A}$, is applied along x-direction and we measure CP of the light propagating along z-axis while biasing one of the LEDs at either side of the p-channel. The occurrence of the SHE upon applying I_p is demonstrated in Fig. 3(b). When biasing, e.g., LED 1, peak B polarization of the light emitted from the region near the corresponding p-n junction step edge is non-zero and its sign, i.e. the sign of $\langle s_z \rangle$ of the holes, flips upon reversing I_p . The detected polarization of 1% represents a lower bound of the SHE induced spin accumulation at the edge because the emitted light intensity decreases only gradually when moving from the biased junction towards the opposite side of the 2DHG channel [20]. To highlight the consistency of the signal with the unique SHE phenomenology, we compare in Fig. 3(c) CPs obtained in experiment where I_p was fixed and either LED 1 or LED 2 was activated. The opposite sign of these two signals confirms opposite $\langle s_z \rangle$ at the two edges, establishing the SHE origin.

To stimulate a detailed microscopic analysis of the observed SHE, including the discussion of the role of disorder, we present in Fig. 3(d) Kubo formula calculations for wafer 1 of the spin Hall conductivity, σ_{SH} , which is derived directly from SO coupled band structure and approaches a disorder independent value in high mobility systems [5, 6, 9]. For the experimental density and for a quasiparticle life-time broadening of 1.2 meV, estimated from the measured mobility of $3400 \text{ cm}^2/\text{Vs}$ and calculated HH effective mass of $0.27 m_e$, the σ_{SH} we obtain is only weakly suppressed by disorder, suggesting that our sample is in the regime referred to as the intrinsic SHE [5, 6]. Note that the robustness of this intrinsic SHE against weak disorder has been challenged by several perturbation-theory analytical studies [11, 16, 17]. However, the well defined clean limit of the SHE has recently been confirmed by numerical quantum transport calculations based on exact eigenstates of the disordered system, by numerical studies utilizing the

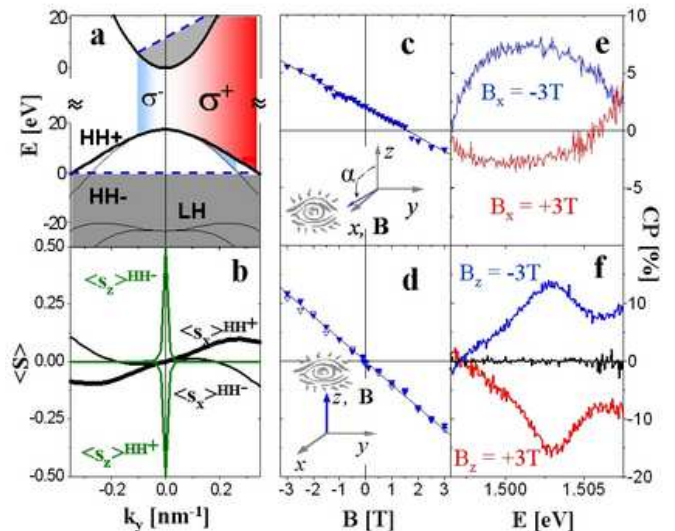


FIG. 2: Spin-polarization in the absence of the SHE driving current. (a) Theoretical energy spectrum of the 2DHG along k_y component of the wavevector (parallel to I_{LED}), of the heavy-hole (HH) and light-hole (LH) subband, spin-split due to the Rashba SO-coupling. Unbiased wafer 1 was assumed in the calculations. Small shift of the subband energies towards the top of the valence band is expected for wafer 2 and under bias. Schematic color plot demonstrates circularly polarized light emission induced by transitions from the asymmetrically occupied conduction band to the HH+ subband. (b) Theoretical spin-polarization components along k_y in the HH+ and HH- subbands. (An infinitesimal magnetic field along z-direction was added to break the degeneracy at $\mathbf{k} = 0$). Except for a small region near $k_y = 0$, spins are oriented in-plane and perpendicular to the k -vector. (c) Circular polarization, defined as the relative difference between intensities of left and right circularly polarized light, plotted as a function of the in-plane magnetic field along the x-axis, measured in wafer 1. The observation angle is $\alpha = 85^\circ$ which is the maximum detection angle allowed in our experimental set-up. The experiment measures, to high accuracy, the x-component of the light polarization vector which is proportional to $\langle s_x \rangle$. (d) Spectral plot of the circular polarization near peak B for field ± 3 T. (e) Same as (c) for magnetic and light detection axis along the normal to the 2DHG plane. (f) Same as (d) for field 0 and ± 3 T. At zero magnetic field the z-component of the polarization vanishes. All measurements are done at 4.2 K.

Landauer-Buttiker scattering formalism [13, 14, 18, 19]. In addition, recent analytical calculations corresponding to our 2DHG confined in an asymmetric quantum well have shown that the vertex corrections due to impurity scattering vanishes in this system, supporting the robustness of the intrinsic SHE in the presence of weak disorder scattering in this system [25]. Experimental exploration of the phase diagram in Fig. 3(d) will help to establish the role of disorder in the observed effect.

We conclude by noting that, beside the demonstrated ability to induce and detect spin-polarization in the ab-

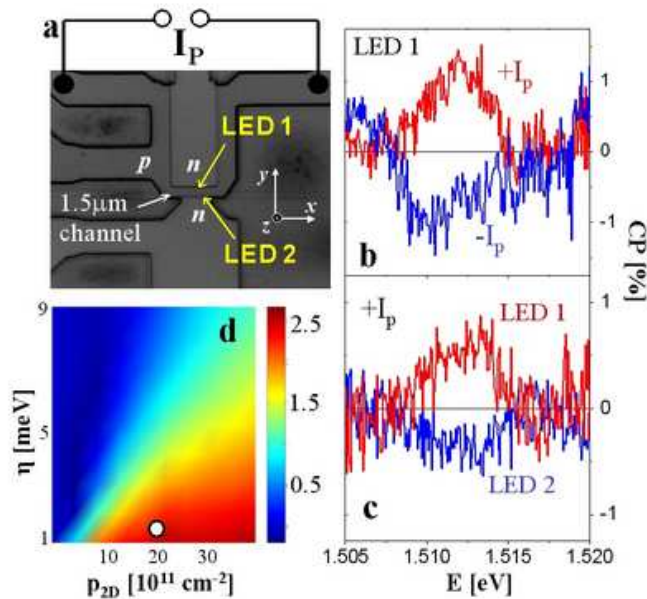


FIG. 3: SHE experiment. (a) Scanning electron microscopy image of the SHE LED device. The top (LED 1) or bottom (LED 2) n-contacts are used to measure the EL at opposite edges of the 2DHG p-channel parallel to the SHE driving current I_p . (b) Polarization along z-axis measured with active LED 1 for two opposite I_p current orientations. Spectral region of peak B of the high bias EL curve of wafer 1 is shown. Non-zero and opposite out-of-plane polarization for the two I_p orientations demonstrates the SHE. (c) Polarization along z-axis measured with fixed I_p current and for biased LED 1 or LED 2. The data show opposite polarizations at opposite edges of the 2DHG channel confirming the SHE origin of the measured signal. (d) Theoretical intrinsic SHE conductivity in units of $e/8\pi$ vs. quasiparticle life-time broadening and 2D hole density. Parameters corresponding to our 2DHG, indicated by a white dot, fall into the strong intrinsic SHE part of the theoretical diagram.

sence of external magnetic fields, our novel planar design allows the fabrication of more complex microdevices that integrate on a single semiconductor chip these two functionalities with transmission of the spin information between different parts of a device. Lithographically defined gate electrodes may provide additional control of the SHE, and therefore of the overall device performance, by varying 2DHG density or SO coupling.

Note added: After our work, on which this Letter is based on, was completed and presented at the Gordon Research Conference on Magnetic Nanostructures (Big Sky, Minnesota, August 2004) and at the Oxford Kobe Seminar on Spintronics (Kobe, Japan, September 2004) an independent experimental observation of the SHE has been reported [26]. We point out that these two exper-

iments are in very different regimes, ours being in the strong SO coupled regime in which the SO splitting is larger than the disorder broadening, and the samples in Ref. 26 in the weak SO coupled regime.

We thank Mohamed N. Khalid, Allan H. MacDonald, and Shoucheng Zhang for many useful discussions. The work was supported by Grant Agency of the Czech Republic through Grant 202/02/0912.

-
- [1] R. E. Prange, and G. M. Girvin, *The Quantum Hall Effect* (Springer-Verlag, New York, 1990).
 - [2] *The Hall Effect and Its Applications* (eds Chien, C.L. and Westgate, C.R.) (Plenum, New York, 1980).
 - [3] M. I. Dyakonov, and V. I. Perel, *Phys. Lett. A* **35**, 459 (1971).
 - [4] J. E. Hirsch, *Phys. Rev. Lett.* **83**, 1834 (1999).
 - [5] S. Murakami, N. Nagaosa, and S.-C. Zhang, *Science* **301**, 1348 (2003).
 - [6] J. Sinova, D. Culcer, Q. Niu, N. A. Sinitsyn, T. Jungwirth, and A. H. MacDonald, *Phys. Rev. Lett.* **92**, 126603 (2004).
 - [7] J. Hu, B. A. Bernevig, and C. Wu, *Phys. B* **17**, 5991-6000 (2003).
 - [8] E. I. Rashba, *Phys. Rev. B* **68**, 241315 (2003).
 - [9] J. Schliemann, and D. Loss, *Phys. Rev. B* **69**, 165315 (2004).
 - [10] S.-Q. Shen, *Phys. Rev. B* **70**, 081311 (2004).
 - [11] J. Inoue, G. E. Bauer, and L. W. Molenkamp, *Phys. Rev. B* **70**, 041303 (2004).
 - [12] N. A. Sinitsyn, E. M. Hankiewicz, W. Teizer, and J. Sinova, *Phys. Rev. B* **70**, 081312 (2004).
 - [13] L. Sheng, D. S. Sheng, C. S. Ting, cond-mat/0409038.
 - [14] B.K. Nikolić, L. P. Zárbo, and S. Souma cond-mat/0408693.
 - [15] J. Schliemann, and D. Loss, cond-mat/0405436.
 - [16] E.G. Mishchenko, A.V. Shytov, B.I. Halperin, cond-mat/0406730.
 - [17] R. Raimondi, and P. Schwab, cond-mat/0408233.
 - [18] K. Nomura, J. Sinova, T. Jungwirth, Q. Niu, and A. H. MacDonald, cond-mat/0407279.
 - [19] E.M. Hankiewicz, L.W. Molenkamp, T. Jungwirth, and J. Sinova, cond-mat/0409334.
 - [20] B. Kastner, cond-mat/0411130.
 - [21] W. Ossau, E. Bangert, and G. Weimann, *Solid State Commun.* **64** 711 (1987).
 - [22] A. Y. Silov, et.al. *J. Appl. Phys.* **73**, 7775 (1993).
 - [23] R. Winkler, *Springer Tracts in Modern Physics* 191 (Springer-Verlag, Berlin, 2003).
 - [24] A. G. Mal'shukov, and K. A. Chao, *Phys. Rev. B* **65**, 241308 (2002).
 - [25] A. Bernevig and S.-C. Zhang, private communication.
 - [26] Y.K. Kato, R.C. Myers, A.C. Gosard, and D.D. Awschalom, *Scienceexpress*, <http://www.scienceexpress.org>.